Accepted Manuscript published in *Electrochimica Acta*
10.1016/j.electacta.2022.140750

Tuning Cationic Transport in NiSalen Polymers via Pseudo-Crown Functionality

Alexey I. Volkov [a], Rostislav V. Apraksin [b], Egor A. Falaleev [a], Julia V. Novoselova [a], Yulia A. Volosatova [a], Daniil A. Lukyanov [a], Elena V. Alekseeva [a], Oleg V. Levin [a]*

[a] Institute of Chemistry, St. Petersburg State University, 7/9 Universitetskaya nab., St. Petersburg, 199034, Russia

[b] Ioffe Institute, 26 Politekhnicheskaya str., St. Petersburg, 194021, Russia

*o.v.levin@spbu.ru

Abstract

Polymeric films based on nickel complexes with salen-type ligands have received considerable attention recently owing to electrocatalytic, electrochromic, and charge storing properties. The latter makes them suitable metal-organic materials for electrochemical power sources, i.e., batteries and supercapacitors. Optimization of the properties of electrode materials is closely linked to the understanding of charge storage mechanisms. The introduction of CH_3O substituent into the molecule results in peculiar ionic transport mechanism, owing to the possibility of alkaline ions coordination.

Here we study the recharging mechanism of poly[Ni(CH_3Osalen)] films in various electrolyte solutions. In presence of alkali ions, the electronic effects of methoxy substituent provide mixed anionic and cationic charge compensation mechanism, as cations reversibly coordinate to the present pseudo-crown functionality. By applying the combination of XRD, CV/EQCM and EIS methods to the film in electrolytes containing Li^+, Na^+, K^+, and Et_4N^+ cations, and BF_4^-, ClO_4^- and bistrifluoromethanesulfonimidate ($TFSI^-$) anions, we propose a model that describes the ionic transport in such polymeric films and allows to estimate the anionic and cationic contribution to the total amount of transferred species during charging and discharging.

Keywords

Nickel salen complexes; electroactive polymers; electrochemical quartz crystal microbalance; ionic transport; pseudo-crown ether

1. Introduction

Conductive polymers based on metal-salen (salen = (N,N'-ethylenebis(salicylimine)) complexes attract considerable attention since their first inception in 1989 [1]. A significant advantage of the polymers based on metal complexes is ease of alteration of their electronic and chemical properties by modifying the ligand structure [2] and selecting different metal centers [3]. The polymeric nickel complexes with salen-type ligands (poly[Ni(*salen*)]) are known for their electrochemical activity, mechanical stability, as well as low cost, availability, and ease of chemical modification [4]. Like other intrinsically conducting polymers, poly[Ni(*salen*)] complexes show electrical conductivity [5]. This leads to extensive study of such materials in sensors [6,7] and electrochromic devices [8].

Lithium-ion batteries are one of the most advanced types of energy storage devices to date. Currently, they overwhelmingly employ inorganic active materials, yet organic ones are viable contenders. A whole area of research focuses on organic batteries cathodes, anodes, and electrolytes suitable for them [9]. Recently, the possibility of using poly[Ni(*salen*)]-based materials in lithium-organic batteries has garnered much interest [10–12], in no small part owing to introduction of redox-substituents which allows to increase the specific capacity of the material to the values that are relevant in practice [12].

The success of poly[Ni(*salen*)] application in materials for energy storage and conversion devices depends on understanding of their recharging mechanisms. Radical cations form during oxidation of these materials, which require charge compensation by intercalation of the anion from the electrolyte (Scheme 1). Thus, the redox processes in polymers synthesized from

tetraalkylammonium salts are usually accompanied by anionic transport [13,14]. Yet currently there is no in-depth study of recharging mechanisms of poly[Ni(*salen*)] films in electrolytes with alkaline cations, which is essential for application in metal-ion batteries.

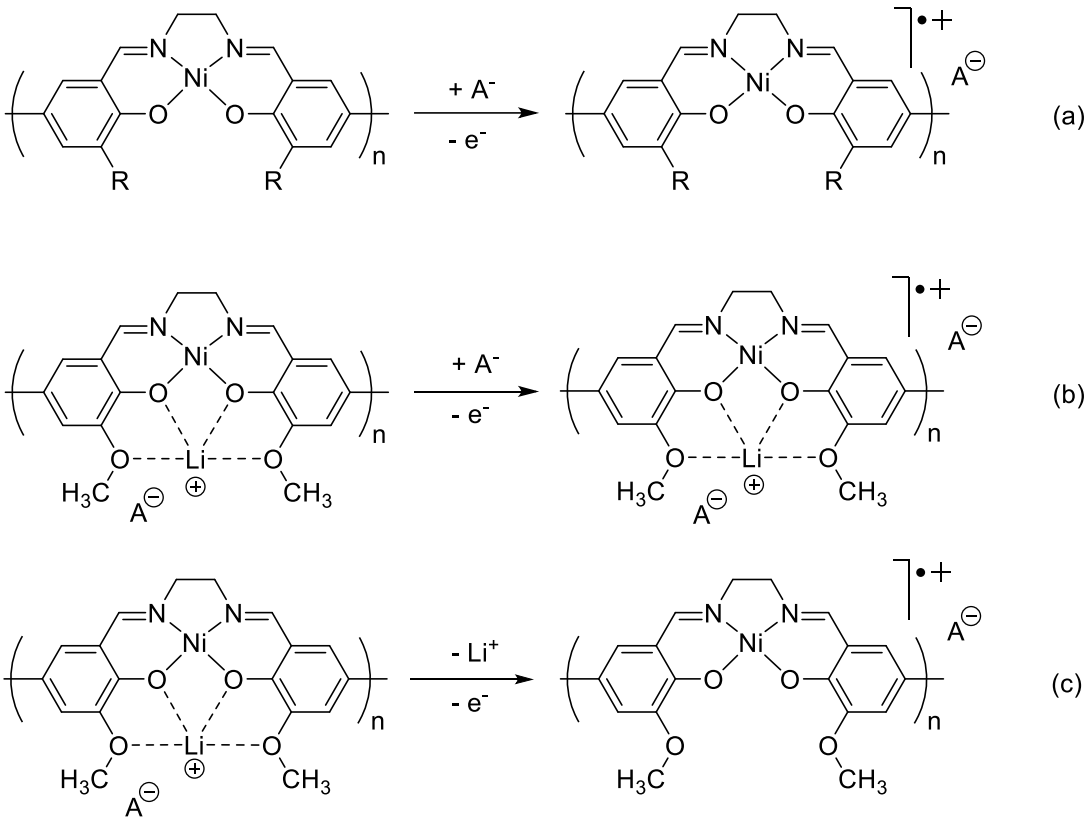

Scheme 1. Charge compensation mechanisms for p-doped poly[Ni(Rsalen)] fragments: a) anionic doping of the oxidized fragment, typical for conducting polymers; b) anionic doping of poly[Ni(CH_3Osalen)] fragment with strongly coordinated Li^+; c) cationic de-doping of poly[Ni(CH_3Osalen)] fragment via elimination of Li^+.

In most cases, only one type of ions—cations or anions—can compensate the charge of specific electrode material in set conditions. Typically, commercially available batteries consist of graphitic anode and inorganic cathode [15], which all can accommodate Li^+ ions, making it the sole transport species. Conversely, anions (A^-) are often dopant species in organic polymer cathodes, as oxidation of the neutral form produces cation radicals, i.e., positively charged species. Therefore, Li-doped

anode (e.g., graphite, alloy, or lithium) and anion-doped cathode (e.g., polypyrrole) deplete the electrolyte of both cations and anions. This requires addition of excess of electrolyte to provide enough Li^+ and A^- for electrode reactions and ensure ionic conductivity, decreasing total energy density of the cells [9]. Thus, studying ion transport processes in organic cathodes and finding conditions which ensure cationic transport are vital tasks.

Electrochemical quartz crystal microbalance (EQCM) [16,17] is a valuable instrument for studying ion transport processes. It allows to monitor mass changes during polymer cycling between neutral and doped states. Several research groups have investigated the issue of ionic transport in the films of electrochemically active polymers [13–19]. Usually, anions act as charge-compensating ions for p-doped (oxidized) conducting polymers [20]. EQCM proved particularly useful for studying polypyrrole systems, yielding the following aspects that affect doping mechanisms. Dziewoński et al. point out the following factors that affect the mode of transport: porosity of the polymer layer, polymerization solvent, cycling solvent, nature of counter ions, and thickness of polymer layer [21]. The difference in the charge [22] or size [23] of the counter ion may have a determining role in the mode of ionic transport for otherwise identical systems.

The research of charge transport in polyaniline films [24] highlighted the fact that molar mass of cations is usually one to two orders magnitude less than that of anions, which makes deducing the underlying processes from EQCM results more complex, especially in the case of mixed transport. When protons or lithium ions are the charge carriers in electrochemical systems, this obstacle is particularly significant. In such cases, even the solvent movement during recharging may have larger mass flux contribution than Li^+ transport, thus skewing the measured values and affecting conclusions.

Existing evidence for poly[Ni(*salen*)] films supports the mechanism in Scheme 1b. With two -OCH_3 groups in close proximity to the chelation cavity of the *salen* ligand, an additional *pseudo*-crown

chelation cavity appears, which is highly capable of coordinating the alkali metal ion. Hillman et al. showed that this effect leads to the peaks shift and the change of the shape of the cyclic voltammogram (CV) of methoxylated poly[Cu(*salen*)] films [3].

Similar coordination of lithium atoms to oxygen in [M(*salen*)] single crystals was also detected by X-ray diffraction (XRD) method [25–27]. X-ray photoelectron spectroscopy (XPS) studies performed for poly[Ni(R*salen*)] films also revealed lithium presence [4]. Notably, lithium contents varied for oxidized and reduced forms of the polymer. This allowed authors to conclude that lithium ions movement takes part in charge compensation, however, low sensitivity of XPS method for Li element led to inaccuracy in calculation of exact lithium atomic percentage, thus rendering the method too imprecise for exact lithium contents detection. On the other hand, XPS of methoxylated poly[Ni(R*salen*)] film after contact with $Ba(ClO_4)_2$ showed unambiguous pseudo-crown coordination of the cation [27].

The reported data suggests that in the presence of oxygen-containing substituents in the polymer structure the alternative to anionic doping mechanism exists. The expulsion of the cation coordinated to oxygen atoms (Scheme 1c) may compensate the charge during the oxidation of the polymer. Such mechanism would ensure cationic transport during oxidation and reduction of the films. Indeed, in our earlier work we showed the switching of the ionic transport to a Li^+ mode by introducing an anchoring anion—poly(styrenesulfonate)—into poly[Ni(CH_3Osalen)] structure [28]. The next step is studying the mechanism of charge compensation in pristine poly[Ni(CH_3Osalen)] films without introduction of the negatively charged polymer.

In this work we studied poly[Ni(CH_3Osalen)] polymeric complexes in background electrolytes with ions of various nature. To do this, we selected supporting electrolytes that contained species with diverse sizes, mobility, and nature from the pool of Li^+, Na^+, K^+, and Et_4N^+ cations, and BF_4^-, ClO_4^-, bistrifluoromethanesulfonimidate ($TFSI^-$) anions. We deposited the

poly[Ni(CH_3Osalen)]films and studied the mechanisms of charge compensation in the obtained films in respective electrolytes using operando CV/EQCM method that allows to monitor the current and mass change responses simultaneously. Based on the obtained data, we determined the mechanisms of the dopant species transport in polymer films and devised the models that allow to estimate contributions of anionic and cationic transport at each stage of polymer film charging/discharging. Additional studies by electrochemical impedance spectroscopy (EIS) supported operando CV/EQCM data. To study the coordination modes of the alkali metal cations with the unit of the polymer, we have determined the structures of the monomeric Ni(CH_3Osalen) crystallized with these cations, and thus confirmed possibility of alkaline cations coordination within [Ni(CH_3Osalen)]. Finally, we outlined the conditions, i.e., electrolyte composition and ligand structure, necessary to ensure either anionic or mixed charge transport. This study provided an important opportunity to advance the understanding of the link between the nature of cations and anions in the electrolyte and the charge compensation mechanism.

2. Materials and methods

2.1. Chemicals

[Ni(CH_3Osalen)] and [Ni(CH_3salen)] (Scheme 2) were prepared as described in the literature [29]. Anhydrous $LiClO_4$ was dried at 120 °C to constant weight before use. LiTFSI, $LiBF_4$, $NaBF_4$, KBF_4, tetraethylammonium tetrafluoroborate (Et_4NBF_4), $AgNO_3$, and acetonitrile (AN) (HPLC grade) were used without further purification.

Accepted Manuscript published in *Electrochimica Acta*
10.1016/j.electacta.2022.140750

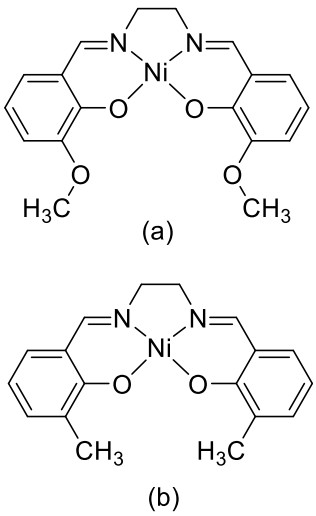

Scheme 2. The structure of [Ni(CH_3Osalen)] (a) and [Ni(CH_3salen)] (b) monomers.

2.2. Electrochemical synthesis and studies

All electrochemical experiments were conducted in Ar-filled glovebox (Vilitek, Russia) using a standard three-electrode cell. Pt spiral (visible surface area ~2 cm^2) was used as a counter electrode, and $Ag/AgNO_3$ electrode (5 mmol dm^{-3} $AgNO_3$, 0.1 mol dm^{-3} $LiClO_4$ in AN inner solution, 0.4 V vs. Ag/AgCl (sat. NaCl)) was used as a reference electrode. All potential values in the present work are reported relative to $Ag/AgNO_3$ electrode. The working electrode choice depended on a method used: Ti/Pt plated quartz crystal for operando CV/EQCM, and glassy carbon electrode for EIS studies.

*2.2.1. Poly[Ni(*salen*)] films synthesis*

Electrochemical signals were recorded on an Autolab PGSTAT302N potentiostat. In the case of operando EQCM studies gravimetric response from QCM200 Quartz Crystal Microbalance (Stanford Research Systems) was obtained simultaneously with current response in cyclic voltammetry.

The poly[Ni(CH_3Osalen)] polymer films were deposited on a surface of working electrode by cycling the applied potential between −0.15 V and 0.9 V at 50 mV s^{-1} scan rate in 1 mmol dm^{-3}

monomer solution in AN with 0.1 mol dm^{-3} $LiBF_4$, $NaBF_4$, KBF_4, $LiClO_4$ or LiTFSI or as supporting electrolytes. The films were then thoroughly washed with AN and dried *in vacuo*.

We further denote the polymeric films in the manner poly[Ni(CH_3Osalen)]/*electrolyte*, where *electrolyte* is the background electrolyte used for synthesis and electrochemical studies of the film.

Additionally, poly[Ni(CH_3salen)]/LiTFSI film has been synthesized using the same procedure for comparison.

2.2.2. Electrochemical quartz crystal microbalance (EQCM)

Operando CV/EQCM studies of polymeric films were performed on a Ti/Pt plated quartz crystal (5 MHz, piezoactive area 1.37 cm^2). The quartz resonance frequency was registered as an analog signal with a 200 Hz V^{-1} resolution. The films were usually synthesized for several CV cycles to obtain thin rigid films to accommodate the conditions suitable for application of the Sauerbrey equation. The cell was filled with 0.1 mol dm^{-3} the same background electrolyte as the one used for the deposition of each film. To ensure reproducibility of the data, the potential was cycled at 50 mV s^{-1} between −0.3 V and 0.9 V until stable CV and mass-voltage curves were reached, i.e., cycle-to-cycle changes in response were minimal.

Sauerbrey equation allows to calculate the mass change (Δm) from the shift of resonance frequency (Δf) (Eq. 1).

$$\Delta f = \frac{-2f_0^2}{A\sqrt{\rho_q \mu_q}} \Delta m \qquad \text{Eq. 1}$$

Here, f_0 is oscillation frequency of the fundamental mode of the quartz crystal, A is the crystal area (1.37 cm^2), ρ_q is density of quartz (2.648 g cm^{-3}) and μ_q is shear modulus of quartz ($2.947 \cdot 10^{11}$ g cm^{-1} s^{-2}). These values are specific for the device, and in this case may be substituted (Eq. 2) with the sensitivity factor C_f (56.6 Hz μg^{-1} cm^2).

$$\Delta f = -C_f \Delta m \quad \text{Eq. 2}$$

Whenever the flux (M, g mol^{-1}) of the particles is discussed in the context of transport, we used Faraday's law of electrolysis (Eq. 3) to calculate M value from the average slopes of linear segments of Δm–Q plots obtained using operando EQCM.

$$M = \frac{\partial m}{\partial Q} zF = kzF \quad \text{Eq. 3}$$

Here, zF is the charge carried per mole of species measured as the electron flux at the electrode/polymer interface, thus is positive on oxidation [30], and is considered to be faradaic-only, i.e., ignoring double layer effects. The sign of M is defined by the value of $\partial m/\partial Q$, which may be calculated as a derivative from the linear sections of Δm–Q plots, so it may be substituted with k (g C^{-1}) slope value here.

2.2.3. Electrochemical impedance spectroscopy (EIS)

For EIS the polymer films were potentiodynamically synthesized on a 0.07 cm^2 glassy carbon electrode by cycling in −0.15 V to 0.9 V potentials range at 50 mV s^{-1} scan rate until the charge passed on reduction was 4 mC. After the synthesis, the electrodes were cycled in the monomer-free solution to stabilize the system response. The EIS measurements were performed in 0.1 mol dm^{-3} $LiBF_4$, $NaBF_4$, and KBF_4 in AN solutions. Before recording spectra, the films were conditioned by applying the desired base potential for 50 s to reach steady state. The spectra were recorded in the frequency range from 100 kHz to 100 mHz. 8 points per decade were recorded, and the applied amplitude was 5 mV rms. One CV cycle was recorded each time between the spectra at different potentials.

2.3. Structure and morphology characterization

Single crystals of [Ni(CH_3Osalen)] were obtained from 0.1 mol dm^{-3} solution of $LiBF_4$ or KBF_4 in AN saturated with [Ni(CH_3Osalen)] monomer. The solution-bearing vial cap was then punctured

with a needle to allow slow evaporation of the solvent and the vial was left at room temperature for several weeks until single crystals formed. Crystallographic studies were performed on an Agilent Technologies (Oxford Diffraction, USA) "Xcalibur" single crystal diffractometer equipped with monochromated MoKα source at 100 K. Additional characterization of selected samples with SEM is presented in Supporting Information, and Crystal Data file is attached separately (also see CCDC numbers 2178147 and 2147958).

2.4. Data analysis and visualization

The obtained data were analyzed using Autolab NOVA 2.1.5 software, further analysis and plotting were performed using OriginPro 9.0. The scientific colormap *batlow* [31] is used in this study to prevent visual distortion of the data and exclusion of readers with color vision deficiencies [32].

3. Results and discussion

3.1. Electrochemical deposition

Ligand structure and electrolyte composition strongly affect the electropolymerization process. Changing the cation, while leaving other parameters intact, results in significant changes both in the shape of voltammograms and the rate of the film growth. The deposition went on until the accumulated charge passed through the cell was 4 mC (or ~3 mC cm^{-2}). This way all obtained films had similar electrochemical activity, while simultaneously satisfying the conditions of Sauerbrey equation validity in terms of low motional resistance (R_m) values. The applicability conditions were derived from the QCM200 operation and service manual [33]. We calculated the R_m value from the recorded conductance voltage (V_c (V)) value using Eq. 4, and since the values were both within the 5000 Ω limit of the device and were generally in the 220–280 Ω range, which is lower than the 400 Ω value for pristine crystal in water (hence the systems are even more rigid). The resistance fluctuated by no more than ±10 Ω within the experiments (<5% of the absolute value), thus the

Sauerbrey equation was deemed applicable. The exact R_m response of each film is presented in Figure S2.

$$R_m = 10000 \cdot 10^{-V_c/5} - 75\ \Omega \qquad \text{Eq. 4}$$

For BF_4^- salts with alkali cations (Figure 1a–c), the number of cycles needed to obtain films with similar activity correlates with the atomic mass of the cation. For Li^+, Na^+, and K^+, the onset potential of electropolymerization is at ~0.6 V, which relates to the only major oxidation process on the first cycle. Monomer oxidation should precede polymerization [8,34], and these processes occur in quick succession, hence there is no peak separation. The peak potential (E_p) differs slightly. For $LiBF_4$, its value on the first cycle is 0.86 V, and it shifts to 0.79 V on the second cycle. The CVs of films synthesized in both $NaBF_4$ and KBF_4 solutions do not feature a resolved peak on the first cycle, and the following cycles suggest the polymer oxidation peak located at ca. (0.85–0.9) V [8,34]. Though the anodic peaks are not fully resolved, we did not expand the range to the more positive potential, as the films are subject to irreversible oxidation there. Reduction sweep in each case contains three peaks. Their exact locations are difficult to define, as they differ depending on both the cation and cycle number. The peak at ca. (0.55–0.6) V relates to substrate adsorption of species present in the solution [35]. While very clearly pronounced for electrolyte with Li^+, it is less visible in the case of K^+, as the shape of the voltammogram is the most capacitor-like in this case. The process at ca. (0.35–0.45) V is reduction of the formed film, paired with oxidation at ca. (0.4–0.55) V. This is by far the most intense process in all three electrolytes. The third shallow peak is at ~0.20 V, which indicates the second step of polymer film reduction, which is then oxidized at ca. (0.3–0.4) V [36].

In contrast to alkali metal ions, in the electrolyte with Et_4N^+ cation the film grows faster (Figure 1d). Here a single cycle is enough to obtain the film of desired electrochemical activity. The monomer oxidation process onset is at ~0.55 V, and, contrary to previous examples, the polymerization peak

is well-resolved, with E_p = 0.63 V. Reduction peaks at 0.45 V and −0.36 V are sharper than those in alkali metal ions-based solutions. The peak at 0.56 V, on the other hand, is less pronounced.

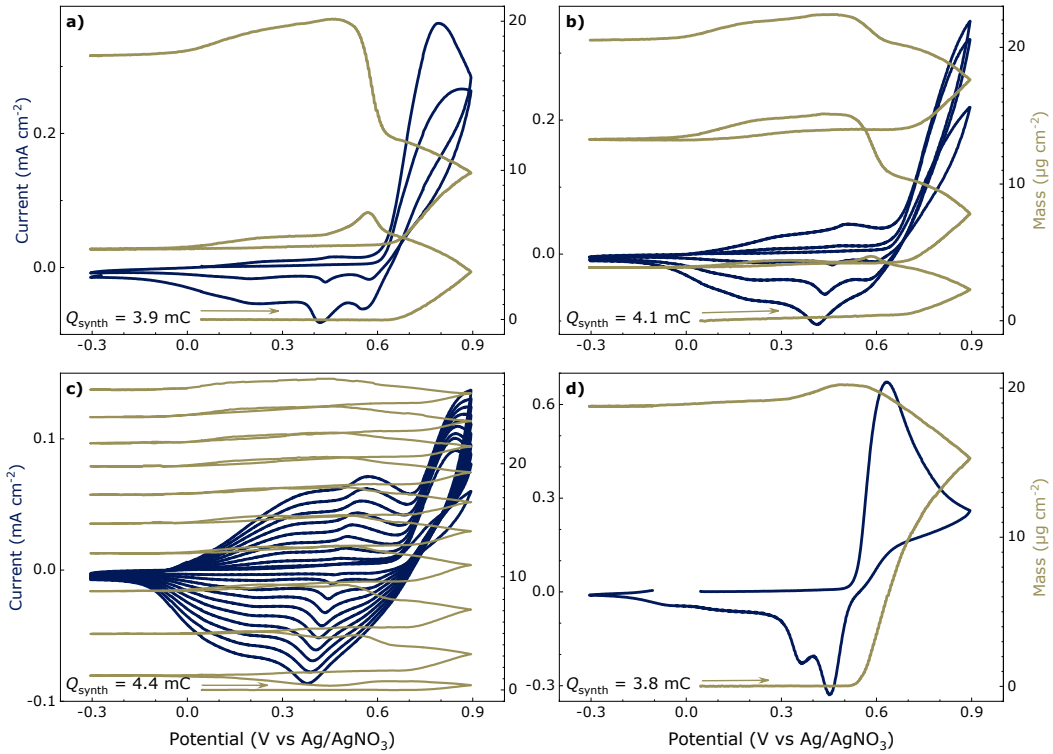

Figure 1. Cyclic voltammograms and mass of poly[Ni(CH$_3$Osalen)] films during electropolymerization from monomer solutions with 0.1 mol dm^{-3} BF_4^- salts and various cations: a) Li^+, b) Na^+, c) K^+, d) Et_4N^+.

We electrodeposited another set of polymers using salts with Li^+ cation and different anions (Figure 2). The most common mass loading for films deposited in preceding syntheses was ~20 µg cm^{-2}, so we attempted to maintain this trend. This required a total charge of 7.1 mC to obtain a 19 µg cm^{-2} film from the $LiClO_4$ solution. During the synthesis of a 6 µg cm^{-2} film from LiTFSI solution an even higher charge of 14.8 mC was consumed. We did not continue the synthesis in this case, as the R_m for thicker films indicated an increase of the viscoelastic contribution to the resonant frequency of the crystal, which could introduce errors in the following measurements.

The shapes of the cyclic voltammograms are similar to those synthesized from BF_4-based electrolytes. For every synthesis, mass increase starts upon reaching monomer oxidation onset potential. This additionally confirms peak attribution to oxidative polymerization. Slight mass loss is also present in reverse sweep of every cycle at potentials lower than ~0.55 V. De-doping of the polymer is the reason of this decrease, which exact mechanism we will discuss in the following sections. During the synthesis, one also cannot exclude the possibility of mass loss due to desorption of oligomeric $[Ni(CH_3Osalen)]_n$ species. The mass increase on the reverse half-cycle in the 0.9 V to 0.55 V range indicates ongoing polymerization right up to the rightmost reduction peak, where the polymer reduction begins.

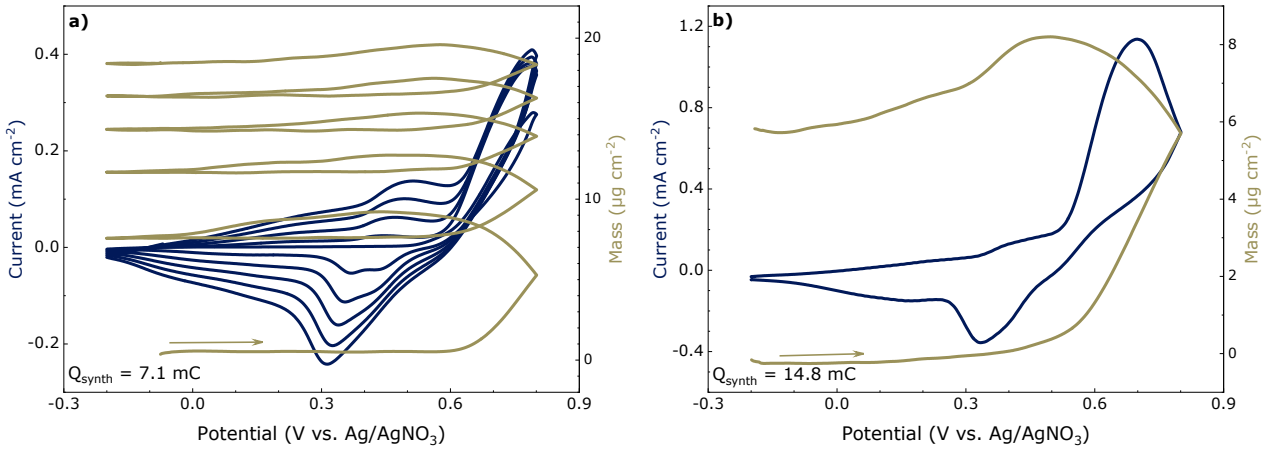

Figure 2. Cyclic voltammograms and mass of poly[Ni(CH_3Osalen)] films during electropolymerization from monomer solutions with 0.1 mol dm^{-3} Li^+ salts and various anions: a) ClO_4^-, b) $TFSI^-$.

The potentials of monomer oxidative polymerization in Table 1 allow to see the intricacies between electrolytes in more detail. For electrolytes with fixed Li^+ cation, there is no link between the peak potential shift and the radius of the anion. For the largest anion, $TFSI^-$, oxidation occurs in the most negative area. Yet, a smaller BF_4^- anion causes the polymerization to shift to lower potentials than a bulkier ClO_4^- anion. This means that other factors, such as the solvation sphere of ions, are at play.

There is also no direct link between cation size and oxidation peak for electrolytes with BF_4^- anions. Here, the lowest oxidation potential is for large Et_4N^+ cation. We may exclude this cation from direct comparison, as it is not a Lewis acid and thus should not coordinate to electron pairs. Yet even alkali metal ions do not have strict order between their radii and oxidation potentials of monomers. The highest oxidation potentials are in the electrolyte with Na^+ ions, and their peak position is difficult to determine, as the peak is located outside of cycling range.

Coordination of the alkali metal ion withdraws electron density, resulting in increase of the oxidation potential. Thus, in the series Et_4NBF_4<$LiBF_4$≈KBF_4<$NaBF_4$ the oxidation potential increases. This is expected of Et_4NBF_4 not to coordinate to O_4 moiety of the complex, while among alkali ions the electron withdrawal effect seems to be the strongest in the case of Na^+.

Table 1. [Ni(CH_3Osalen)] monomer oxidation peaks (E_{ox}, V) depending on the electrolyte composition.

E_{ox} (V)	**BF_4^-**	**ClO_4^-**	**$TFSI^-$**
Li^+ salts	0.79–0.86	0.90	0.70
	Na^+	**K^+**	**Et_4N^+**
BF_4^- salts	>0.90	0.85–0.90	0.63

3.2. Crystal structure

While there are data on structure of various metals complexes with salen-type ligands bearing pseudo-crown functionality in the literature [3,25–27], it is important to confirm whether coordination of alkali ions is possible in the case of compound in the present work. [Ni(CH_3Osalen)]-Li (CCDC 2178147) and [Ni(CH_3Osalen)]-K (CCDC 2147958) single crystals were grown from the saturated monomer solutions in AN, containing either 0.1 mol dm^{-3} $LiBF_4$ or 0.1 mol dm^{-3} KBF_4, respectively. The results (Figure 3a) clearly show that Li^+ coordinates to the

O_4-pseudo-crown functionality present in the molecule. BF_4^- ion compensates the charge. The single crystal structure for [Ni(CH_3Osalen)] with $NaBF_4$ (Figure 3b) was obtained from CCDC [37]. The coordination number of both sodium and potassium (Figure 3c) ions is higher, and thus two [Ni(CH_3Osalen)] molecules attach to them via pseudo-crown functionality, while BF_4^- anion ensures electroneutrality of the system.

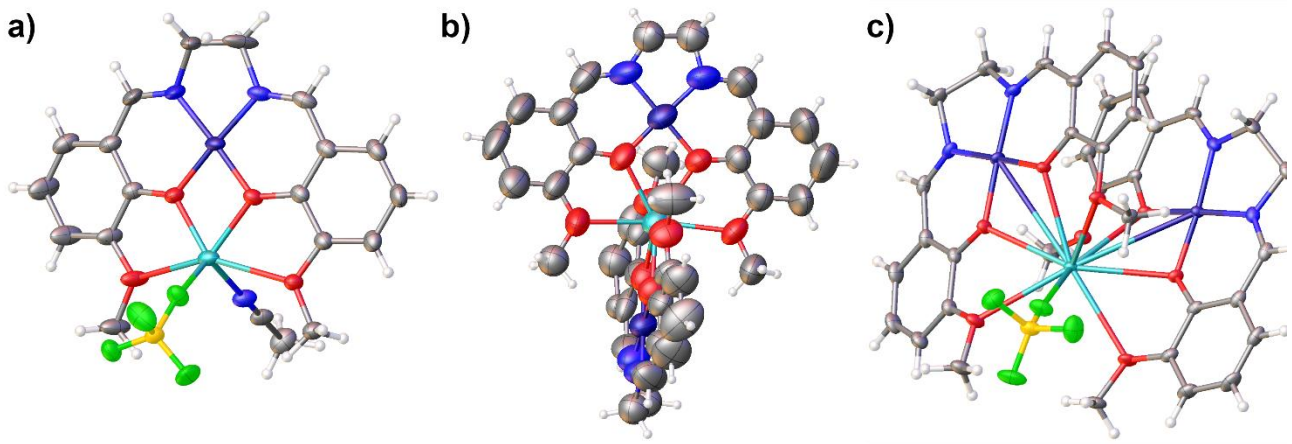

Figure 3. Crystal structures of a) [Ni(CH_3Osalen)]/$LiBF_4$, b) [Ni(CH_3Osalen)]/$NaBF_4$ [37] and c) [Ni(CH_3Osalen)]/KBF_4.

3.3. Cyclic voltammetry and operando EQCM

We recorded EQCM frequency response along cyclic voltammetry measurements, and usually the resulting Q–Δm curve contained two distinct sections, each with its own slope, both on forward and backward scans. We performed linear fitting on each section separately, by averaging the values of oxidation and reduction. Further in text, we use M_1 (g mol^{-1}) for $zF(\mathrm{d}m/\mathrm{d}Q)$ values calculated from the slope of the liner section in negative potential areas of Q–Δm, and M_2 (g mol^{-1}) from the slope in positive potential areas. Further we expand on these trends of electrochemical and mass-transfer response for specific systems and provide a suitable explanation thereof.

3.3.1 Cation variation studies

Cyclic voltammogram of poly[Ni(CH_3Osalen)]/$LiBF_4$ film shows (Figure 4a) three pairs of peaks. The most pronounced oxidation peak appears at 0.54 V, which corresponds to 0.44 V reduction peak. Mass transfer is most intense to the more positive potentials than onset of these peaks, with mass gain on oxidation and mass loss on reduction. The potentials of pairs of peaks both in more positive and negative areas a difficult to estimate as they are too shallow to locate confidently. Nonetheless, in the more positive pair of peaks at ca. (0.7–0.85) V mass gain/loss on oxidation/reduction follows the trend of the major pair of peaks. It is the opposite for the more negative area of the voltammogram at <0.40 V potentials, i.e., positive mass flux is on reduction, and the negative flux is on oxidation. Matching these areas with a Δm–Q plot allows to determine the nature of species participating in the mass transfer processes. We have cycled each film as long as it was reasonable to consider the cycle-to-cycle changes in response minimal. Even though the Coulombic efficiency is about 90% (see Table 2), i.e., the Δm–Q plot would not return to the point of origin, the response is stable when the film is cycled continuously.

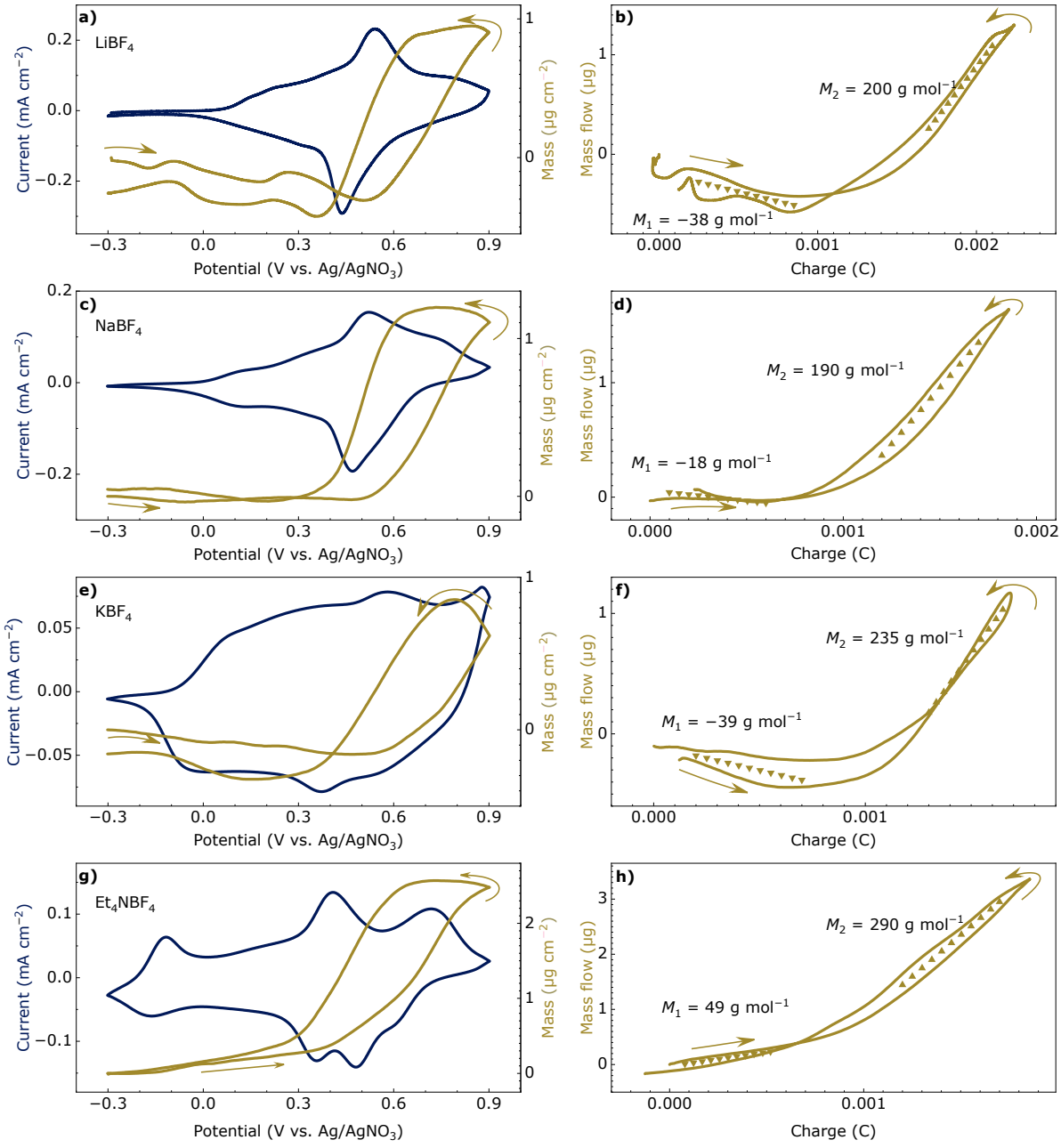

Figure 4. a,c,e,g) CV and Δ*m*–*E* plot for poly[Ni(CH_3Osalen)]/$LiBF_4$ (a), poly[Ni(CH_3Osalen)]/$NaBF_4$ (c), poly[Ni(CH_3Osalen)]/KBF_4 (e), poly[Ni(CH_3Osalen)]/Et_4NBF_4 films. b,d,f,h) corresponding Δ*m*–*Q* plots for the films with estimated average molas mass values.

The calculated M_2 values in most cases are more than 200 g mol^{-1}, exceeding the molar mass of BF_4^- anions (87 g mol^{-1}) expected as dopant-ions upon oxidation, as per Eq. 4. The discrepancy may be explained by solvation of the anion, which is considered further in the discussion.

$$\mathrm{Ni}(CH_3\mathrm{Osalen}) + BF_4^- \overset{-e^-}{\Longleftrightarrow} \mathrm{Ni}(CH_3\mathrm{Osalen})^{\cdot+} \cdot BF_4^- \qquad \text{Eq. 4}$$

For the film cycled in $LiBF_4$, the leftmost pair of peaks is where the mass flow is low, with M_1 value of −38 g mol^{-1}. Again, the negative value aligns well with cationic transport, yet the discrepancy with the 7 g mol^{-1} for Li^+ is discussed further, which is mainly because of low molecular mass of Li^+ (Eq. 5).

$$\mathrm{Ni}(CH_3\mathrm{Osalen}) \cdot Li^+ - Li^+ \overset{-e^-}{\Longleftrightarrow} \mathrm{Ni}(CH_3\mathrm{Osalen})^{\cdot+} \qquad \text{Eq. 5}$$

Inconsistency between the calculated mass of the 200 g mol^{-1} and the expected 87 g mol^{-1} may mean that more particles enter (leave) the film, e.g., solvent molecules accompany anions, increasing the *M* value.

Combined transport of anions, cations and solvent molecules may be represented via a generalized reaction equation:

$$[Red \cdot (C^+A^-)_x \cdot S_z]_{film} \rightleftarrows [Ox^{\cdot+} \cdot C^+_{x-c} \cdot A^-_{x-a} \cdot S_{z-s}]_{film} + cC^+ + aA^- + sS + e^-, \qquad \text{Eq. 6}$$

where *Red* is the reduced fragment of the poly[Ni(CH_3Osalen)] film, and assumed to be an electroneutral quasi-particle capable of one-electron oxidation. $Ox^{\cdot+}$ is its oxidized counterpart, *x* and *z* are the numbers of electrolyte ionic pairs C^+A^- and solvent molecules *S*, respectively, absorbed per one *Red* quasiparticle of polymer; *c*, *a*, and *s* are amounts of cations C^+, anions A^-, and solvent molecules transferring into or out of the polymer film (on oxidation (*reduction*) negative (*positive*) values of these parameters correspond to the inward (*outward*) flux of the species, and positive (*negative*) values correspond to the outward (*inward*) flux).

In this reaction *x* and *z* are arbitrary values, which cannot be estimated from the EQCM method. However, the range of *c*, *a* and *s* values can be found using the charge (Eq. 7) and mass (Eq. 8) balance equations for the reaction Eq. 6:

$$(x - c) - (x - a) + 1 = 0 \qquad \text{Eq. 7}$$

$$-c \cdot M_C - a \cdot M_A - s \cdot M_S = M \qquad \text{Eq. 8}$$

Eq. 7 thus eliminates *x* variable:

$$c = a + 1 \qquad \text{Eq. 9}$$

In Eq. 8, M_C, M_A and M_S are the molar masses of corresponding species, and *M* is either M_1 or M_2 obtained from EQCM data. By solving the system of Eq. 7 and Eq. 8, we obtain:

$$a = -\frac{M + s \cdot M_S + M_C}{M_A + M_C} \qquad \text{Eq. 10}$$

As the solvent flux coefficient *s* is unknown, *a* and *c* may vary in the whole real number range. However, it is reasonable to assume that during oxidation anions should enter the positively charged film and cations should leave it. So, we introduce additional restrictions:

$$a \leq 0 \qquad \text{Eq. 11}$$

$$c \geq 0 \qquad \text{Eq. 12}$$

This restriction does not, however, limit *s* by itself, hence its value can span both over negative and positive numbers, i.e., we are not deliberately choosing inbound or outbound flux of solvent. Instead, equations Eq. 9 through Eq. 12 provide the boundaries for the solvent flow values:

$$-\frac{M+M_C}{M_S} \leq s \leq -\frac{M-M_A}{M_S}. \quad \text{Eq. 13}$$

Hence, for poly[Ni(CH_3Osalen)]/$LiBF_4$ (Figure 4b) with $M = M_2$ = 200 g mol^{-1} per one electron removed, the solution for s is: $-5.1 \leq s \leq -2.8$, where $s = -5.1$ corresponds to pure cationic charge transfer:

$$[Red \cdot (LiBF_4)_x \cdot (CH_3CN)_z]_{film} + 5.1CH_3CN = [Ox^{\cdot+} \cdot (Li^+)_{x-1} \cdot (BF_4^-)_x \cdot (CH_3CN)_{z+5.1}]_{film} + Li^+ + e^-, \quad \text{Eq. 14}$$

and $s = -2.8$ corresponds to pure anionic charge transfer:

$$[Red \cdot (LiBF_4)_x \cdot (CH_3CN)_z]_{film} + BF_4^- + 2.8CH_3CN = [Ox^{\cdot+} \cdot (Li^+)_x \cdot (BF_4^-)_{x+1} \cdot (CH_3CN)_{z+2.8}]_{film} + e^-. \quad \text{Eq. 15}$$

The solution of inequality (Eq. 13) for M_2 for films with BF_4^- shows that anionic flux (M_2) is always accompanied by codirectional solvent flux, as in the $LiBF_4$–$NaBF_4$–KBF_4–Et_4NBF_4 series the allowed $s(M_2)$ values are distributed in −2.5 to −10.2 range. Co-insertion of anions and solvent molecules is a noteworthy phenomenon, as usually in conducting polymers expulsion of solvent occurs on oxidation (in case of, e.g., PEDOT or PANI) [38–40]. However, switching between solvent ingress and egress upon oxidation has also been reported, and the behaviour was linked to presence of both cationic and anionic transport [41]. Nonetheless, the solvent influx along with anions on oxidation has been reported previously for salen-based polymers [13,42], as well as other polymers [43,44]. We presume that the movement of anions along with the solvent should cause significant swelling of the film, as compared to the opposing flows, where the solvent would take place of expulsed anion (and vice versa).

The only common whole number solution (s=−5) for Eq. 13 for BF_4^- anions allows to generalize and assume that upon reduction five AN molecules leave the film along with BF_4^- anions, and we can use this value in calculations. Note that this is not the only solution, as there is a range of

acceptable values of *s*, yet the choice of single common whole-number solution would ease further discussion.

The solutions for $s(M_1)$ for cationic transport (M_1) include s=0, allowing the absence of solvent flow (Table 2). For $NaBF_4$ and KBF_4 (Figure 4d,f), negative M_1 values correlate with the mass of the cation. This suggests that, as in the case of films synthesized from the polyelectrolyte salt [28], the alkali metal cations coordinated to the O_4 fragment of the ligand exit the film on oxidation of the polymer thus compensating the positive charge. The trend does not extend to tetraethylammonium cation, as it is incapable of such coordination. As a result, in Et_4NBF_4 solution the oxidation of the film is accompanied by mass increase from the start, typical for entry of charge-compensating anions. However, for Et_4NBF_4 the M_1 value is less than that of the BF_4^- anion, which may indicate deviations for the *s* value upon the entrance of the anion or a joint anion-cationic charge transport mechanism.

Table 2. Electrochemical properties for each studied system.

	M_1, g mol^{-1}	$s_{min}(M_1)$	$s_{max}(M_1)$	M_2, g mol^{-1}	$s_{min}(M_2)$	$s_{max}(M_2)$	C, F g^{-1}	C_{area}, mF cm^{-2}	Coulombic efficiency, %
$LiBF_4$	−38	0.7	3.0	200	−5.1	−2.8	45	0.80	89
$NaBF_4$	−18	−0.1	2.6	190	−5.2	−2.5	51	1.04	90
KBF_4	−39	0.0	3.1	235	−6.7	−3.6	36	0.95	93
Et_4NBF_4	49	−4.4	0.9	290	−10.2	−5.0	64	1.22	95
$LiClO_4$	−7	0.0	2.6	99	−2.6	0.0	74	1.37	93
LiTFSI	−7	0.0	7.0	150	−3.8	3.2	203	1.18	92

As M_1 values correspond to the molar mass of alkali cations, we do not link *c* and *s* coefficients via equations, rather focusing on anionic transport. Conversely, a solvated BF_4^- anion must enter the

film, and thus we can bind the solvent flow coefficient *s* to the anionic flow coefficient *a* by modifying Eq. 8. Essentially, we assume that the solvation of anions does not depend on the nature of electrolyte cation, so we can exclude one unknown value from the equations linking the solvent flow with anionic flow:

$$-c \cdot M_C - a \cdot (M_A + s \cdot M_S) = M \qquad \text{Eq. 16}$$

With $s = -5$ and *c* linked to *a* via Eq. 9, the solution to Eq. 16 depends only on *M* which can be calculated at any *monotonic* and *semi-linear* segment of Δ*m*–*Q* curve, which excludes transitions from M_1 to M_2 areas. Further we analyze the data for $NaBF_4$ electrolyte to resolve the transport in *non-linear* areas of the Δ*m*–*Q* curve in the cycling range. The solution to the Eq. 16 at each potential produces the dependence of cationic flow (*c*) and anionic flow (*a*) on the stage of the polymer film charging (discharging) (Figure 5b). Cationic transport prevails at lower potentials when the total charge of the film is near zero. As the oxidation goes on, the cationic transport declines, giving way to the increase of anionic transport that overtakes the cationic flow at ca. 0.7 V (Figure 5b). On the reverse scan, the opposite happens: the initial anionic transport via expulsion of BF_4^- anions decreases, and inclusion of Na^+ prevails at ca. 0.4 V.

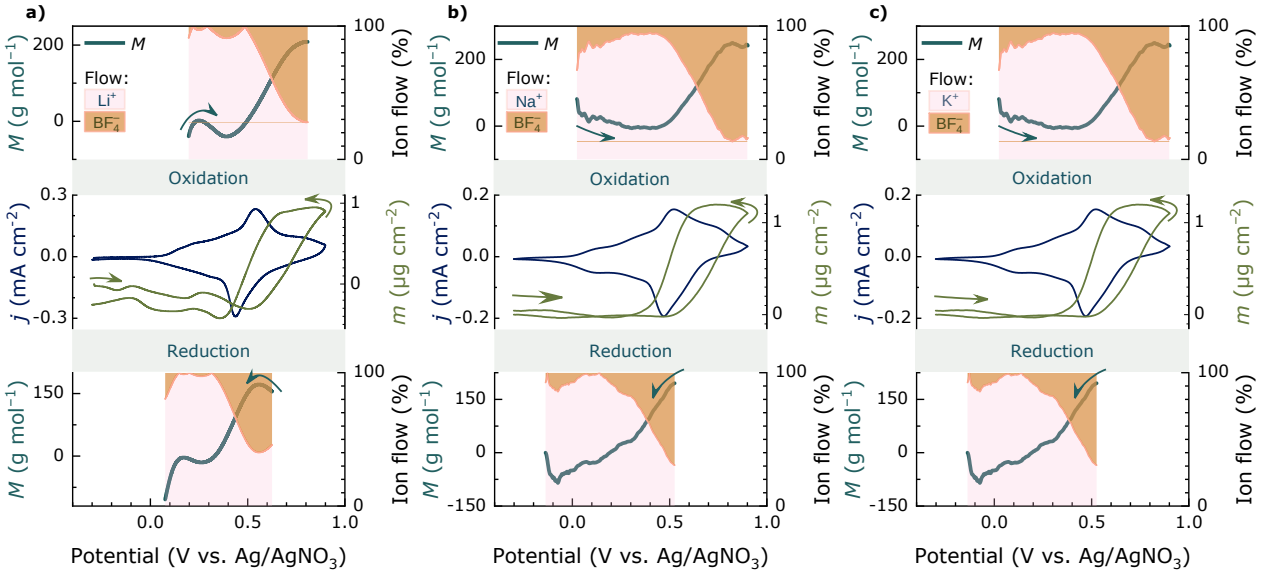

Figure 5. CVs and flux values along the potential axes on oxidation and on reduction, with calculated values for cationic and anionic transport contributions for $LiBF_4$ (a), $NaBF_4$ (b), and KBF_4 (c).

The exact equation—derived from Eq. 16—for the ion flow values presented in Figure 5b, is represented via the molar mass values relevant to $NaBF_4$ in AN, considering Eq. 9 (*a* was substituted with $c-1$):

$$c = \frac{-M + M_A + s \cdot M_S}{M_A + M_C + s \cdot M_S} = \frac{-\frac{\partial m}{\partial Q} + 87 + 5 \cdot 41}{87 + 23 + 5 \cdot 41} = \frac{-\frac{\partial m}{\partial Q} + 292}{315} \qquad \text{Eq. 17}$$

Such representation of ionic flux contributions to total mass transport supplements the general observations of predominantly cationic transport at low charge and predominantly anionic transport at high charge from the common Δm–Q representation in Figure 4d. The calculations hold true for Li^+, Na^+, and K^+ cations (Figure 5a–c), e.g. the alkali ions capable of coordination to O_4 cavity in poly[Ni(CH_3Osalen)]. However, we cannot apply the same reasoning to Et_4N^+ cations (Figure 4g,h), where the molecular mass values calculated from the slope are always positive, because it does not coordinate to O_4 cavity.

As a side note, when we apply Eq. 17 to the lithium, sodium, and potassium series of salts with common BF_4^- anion, the average slopes in "anionic" branch of the $\Delta m–Q$ response yield the following values of c, i.e., cationic transport coefficient: $c_{Li} = 0.31$, $c_{Na} = 0.32$, and $c_K = 0.17$. This may indicate that bulky K^+ has low mobility, compared to Li^+ and Na^+, and thus its flow is less intense than that of smaller cations.

Thus, we have shown that both alkali metal cation transport and anion transport occur during the recharging of poly[Ni(CH_3Osalen)] films in their full electrochemical activity window. However, Et_4N^+ cation showed different behaviour, meaning that the nature of cation affects the extent of applicability of considerations on cationic transport. Meanwhile, this set of experiments was performed only with a BF_4^- anion, yet the choice of anion may also affect the trends of ionic transport in the films. To that end, we performed additional experiments for electrolyte with anion variation.

3.3.2 Anion variation studies

Fixing a Li^+ cation and starting with the ClO_4^- anion that has the closest radius to that of BF_4^-, we have also observed mixed transport (Figure 6). Here we see that M_1 is −7 g mol^{-1}, indicating lithium transport. The remainder of charge (in the >0.4 V potentials area) is characterized by the flux of 99 g mol^{-1}. This is also in line with expectations, as ClO_4^- molar mass is ~99.5 g mol^{-1}. Still, by applying the same set of equations (Eq. 6—Eq. 13), we obtain $-2.6 \leq s \leq 0$, where $s = 0$ is the solution with purely anionic transport, and s = -2.6 corresponds to fully cationic transport. It is likely that a charge carriers switch also occurs here, like in the cases with BF_4^-.

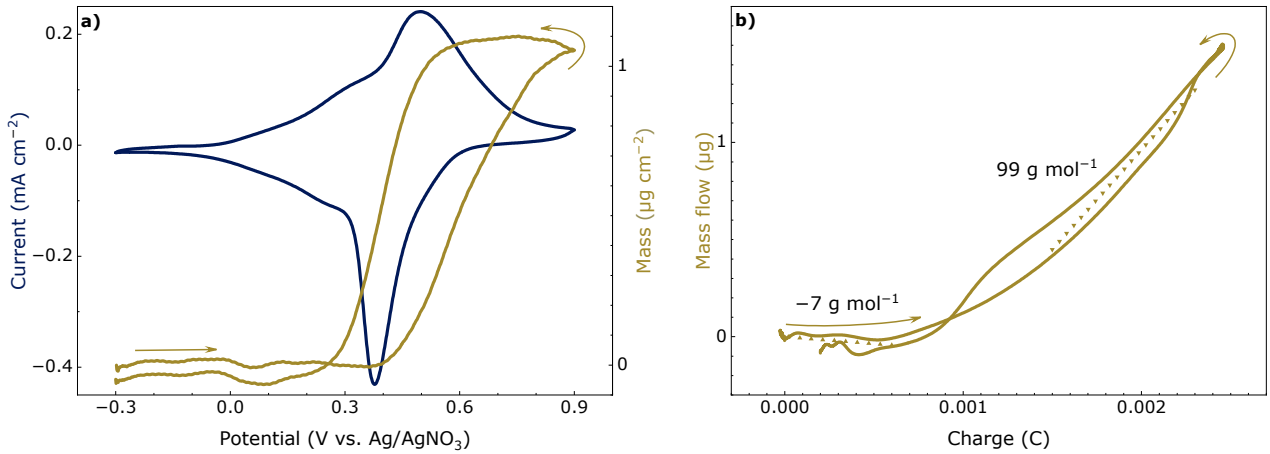

Figure 6. CV and Δ*m*–*E* plot (a) and Δ*m*–*Q* plot (b) for poly[Ni(CH$_3$Osalen)]/LiClO$_4$ film cycled in 0.1 mol dm^{-3} LiClO$_4$/AN.

Then M_1 and M_2 values were also extracted for the films cycled in LiTFSI electrolyte (Figure 7). Bulky TFSI$^-$ anion should support cationic transport as its own movement is limited. Here, the movement of Li$^+$ species also occurs in potentials up to 0.4 V, judging by the average molecular mass of −7 g mol^{-1} in the negative potentials area. The molecular mass value in the positively inclined area of the curve is ca. 150 g mol^{-1}, which is lower than the 280 g mol^{-1} value expected for TFSI$^-$ anions. If TFSI$^-$ is not solvated upon film entry (s=0), the possible cations to anions flow ratio would be 9:11, i.e., c = −0.45, and a = 0.55. Furthermore, if TFSI$^-$ enters the film along with its solvation shell, the cationic contributions would increase even more. There is only a short steep area with ~630 g mol^{-1} value for the completely oxidized film, yet it is difficult to infer a solid explanation for this phenomenon. It is plausible that TFSI$^-$ enters the film with its solvation sphere (8 to 9 molecules of AN) at high oxidation degree, thus causing a significant mass uptake.

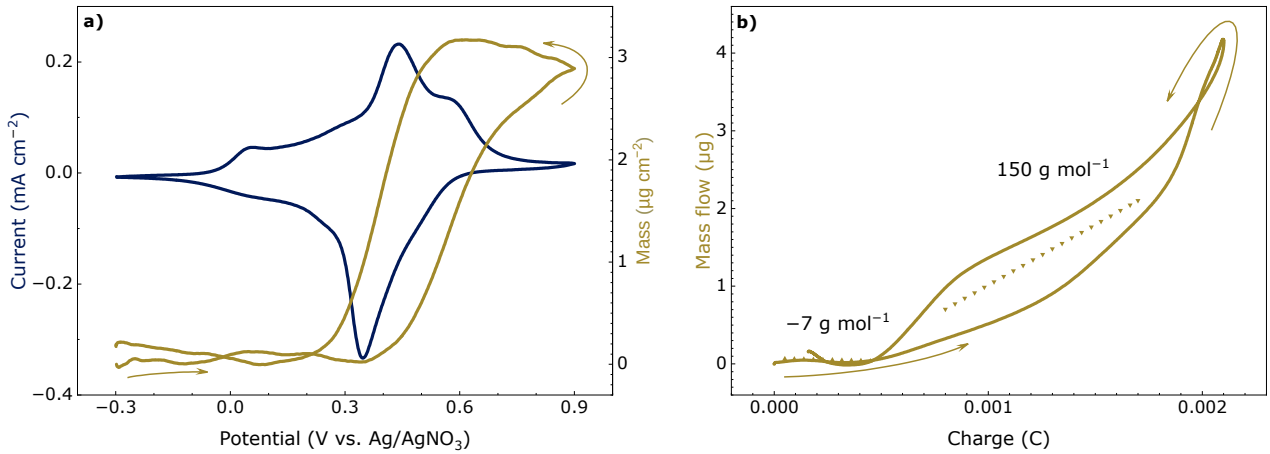

Figure 7. CV and Δ*m*–*E* plot (a) and Δ*m*–*Q* plot (b) for poly[Ni(CH$_3$Osalen)]/LiTFSI film cycled in 0.1 mol dm^{-3} LiTFSI/AN.

These results point unambiguously at co-existing anionic and cationic transport when alkali metals cations are present in the solution, regardless of the choice of the anion. To this point, we assumed that the observed cationic transport is directly caused by alkali cations coordination to O_4 cavity in poly[Ni(CH$_3$Osalen)]. To confirm the crucial role of such coordination in enabling cationic charge compensation mechanism, we employed poly[Ni(CH$_3$Osalen)], which is an analogous polymer with CH$_3$- substituent instead of CH$_3$O-, and thus lacks such a coordination site.

The electrochemical behaviour of poly[Ni(CH$_3$salen)] film cycled in LiTFSI is close to that of poly[Ni(CH$_3$Osalen)], i.e. similar potentials range is available, and similar current values are reached, while there are two pairs of redox peaks at ~−0.01 V and ~0.43 V (Figure 8a). However, Δ*m*–*Q* plot (Figure 8b) shows unambiguous positive slope over whole cycling range, the flux is 362 g mol^{-1}, corresponding to TFSI anions (280 g mol^{-1}) solvated by two AN molecules (2×41 g mol^{-1}). It means that—even in the case of bulky TFSI$^-$ anion—charge compensation during oxidation of poly[Ni(CH$_3$salen)] films proceeds solely with anionic doping. Thus, we show that cationic transport is impossible in this case, and this additionally confirms that CH$_3$O group is a primary driver of cationic transport in poly[Ni(CH$_3$Osalen)] films.

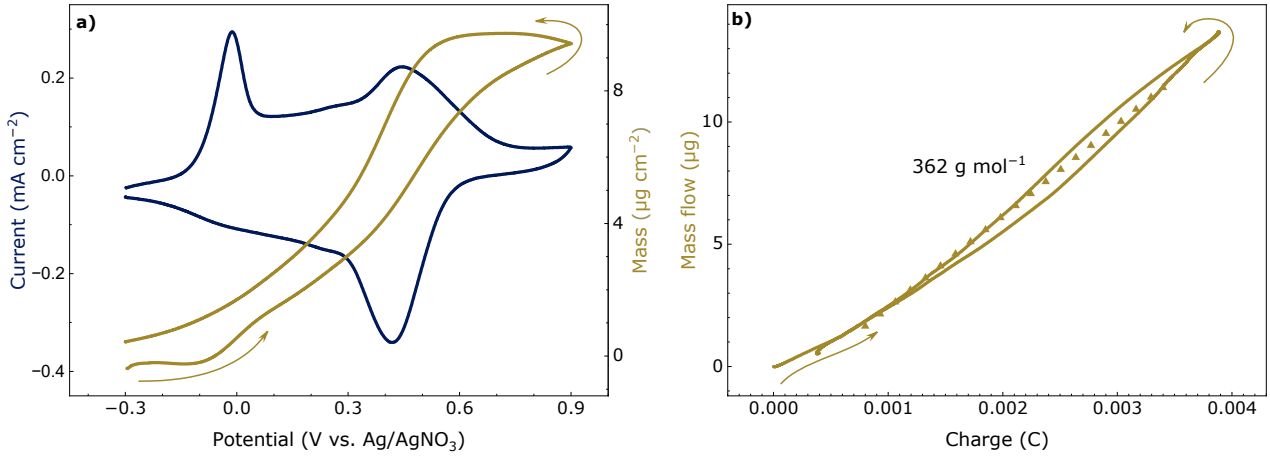

Figure 8. CV and Δ*m*–*E* plot (a) and Δ*m*–*Q* plot (b) for poly[Ni(CH$_3$salen)]/LiTFSI film cycled in 0.1 mol dm^{-3} LiTFSI/AN.

3.4. Electrochemical impedance spectroscopy (EIS)

We performed the EIS of the poly[Ni(CH$_3$Osalen)] in BF_4^--based electrolytes to further study the effect of alkali ion on its contribution to the mass flux. EIS data confirm the observations on the mixed mode of charge compensation. The overall shape of the impedance spectra in Nyquist plots (Figure 9a) is typical for the polymers of this type [45,46]. A short linear Warburg response is observed at the middle frequencies range, and then a capacitance-type response with an angle close to 90° is observed at the low frequencies, which is attributed to the capacitance of the film (C_{lf}).

For the interpretation of impedance data, we used the classical method based on the model by Mathias and Haas [47]. The low-frequency capacitance C_{lf} (Figure 9c) was determined from the slope of the linear portion of the $-Z_{Im}$–ω^{-1} curve (the most representative curves can be found in Figure S4). The calculated capacitance values are in reasonable agreement with the values calculated using cyclic voltammetry data (Table 2). The Warburg constant (σ_w) was calculated as a slope of the mutually parallel linear parts of the (Z_{Re}, $-Z_{Im}$) *vs* $\omega^{-0.5}$ dependencies (the most representative curves are available in Figure S5). The obtained values of σ_w and C_{lf} were used to calculate the binary diffusion coefficient (*D*) by Eq. 18.

$$D = \frac{1}{2}\left(\frac{\left(t_e^2 + t_{ion}^2\right)h}{2\sigma_w C_{lf}}\right)^2, \qquad \text{Eq. 18}$$

Here, t_e and t_{ion} are the electron and dopant ion transfer numbers, here assumed to be equal, so that $t_e = t_{ion} = 0.5$), and h is the thickness of the film (500 nm). The obtained logarithmic values of the binary diffusion coefficient for different potentials are presented in Figure 9b.

The binary diffusion coefficient grows in the $K^+ \rightarrow Na^+ \rightarrow Li^+$ sequence. This agrees with CV/EQCM data which showed that lithium ion is the most mobile one, contributing more to the total mass flux. Other alkali ions contributed less, and their diffusion coefficients decreased accordingly. Upon oxidation, the diffusion coefficients values get closer to one another, regardless of the cation. This is also a direct link to the CV/EQCM observations, which show the predominance of anionic charge compensation at higher potentials.

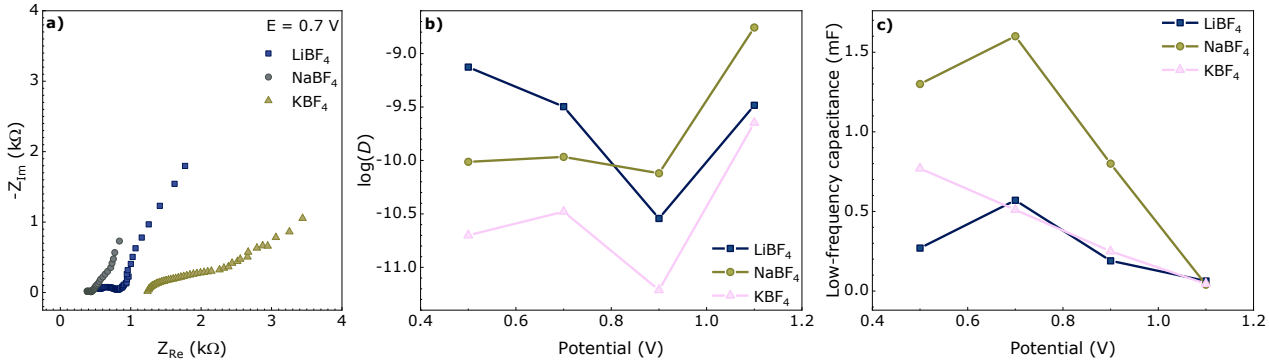

Figure 9. Electrochemical impedance spectra (a), extracted binary diffusion values (b), and low frequency capacitance values (c) for poly[Ni(CH_3Osalen)] films in $LiBF_4$, $NaBF_4$, and KBF_4.

The data obtained using CV/EQCM and EIS methods has long-term implications on the usability of polymeric nickel salen complexes, and especially poly[Ni(CH_3Osalen)], as electrode materials [10]. The specifics of ionic transport matter in systems, where the polymer doping directly triggers the desired phenomenon, such as photogalvanic effect in catalysts [48], or transition into doped

dielectric state in electrode protection layers [49]. The nature of charge-compensating species is especially important in energy storage devices, as the electrolyte should accommodate both electrodes [45,50], and the issue becomes even more urgent when two or more electrode components participate in faradaic processes, e.g., organic radical batteries with nitroxyl pendant groups on a conductive polymeric nickel salen complex backbone [12] or conducting polymer binder in lithium-ion batteries [51]. Thus, we hope this study will provide guidance for proper selection of materials according to desired application.

4. Conclusions

Electrochemical properties of the poly[Ni(*salen*)]-type films change depending on the introduced substituents. We have shown via CV/EQCM that the nature of ionic transport changes significantly upon introduction of the methoxy group into poly[Ni(CH_3Osalen)] films: both cationic and anionic fluxes co-exist during the redox processes in the films, as opposed to anionic-only flux in methyl-substituted poly[Ni(CH_3salen)] films. The phenomenon of cationic transport is apparent for alkaline ions, i.e., lithium, sodium, and potassium, and is caused by O_4 functionality of the complexes, as single crystal structures suggest. At the same time, tetraethylammonium cation does not produce the same effect. In all cases solvent transport accompanies the ionic flux, which we account for in calculations of various species' contribution to the total mass and charge transport. The lack of pseudo-crown functionality results in anionic-only transport for poly[Ni(CH_3salen)] films. Electrochemical impedance spectroscopy data confirm the observations, and further verify that cationic mobility decreases along with the growth of the alkaline ion radius. The spectra also showed the shift of the transport mode to the anionic one upon film oxidation, as diffusion coefficient values in the same-anion different-cation electrolytes approach a common value in the oxidized state.

Acknowledgements

Financial support from RFBR (project no. 20-03-00746) is gratefully acknowledged. Authors thank the Centre for X-ray Diffraction Studies, Interdisciplinary Resource Centre for Nanotechnology, Cryogenic Department of Research Park of SPbSU for performed studies.

References

[1] K.A. Goldsby, J.K. Blaho, L.A. Hoferkamp, Oxidation of nickel(II) bis(salicylaldimine) complexes: Solvent control of the ultimate redox site, Polyhedron. 8 (1989) 113–115. https://doi.org/10.1016/S0277-5387(00)86388-3.

[2] C. Chen, X. Li, F. Deng, J. Li, Electropolymerization and electrochemical behavior of nickel Schiff base complexes with different groups between imine linkages, RSC Advances. 6 (2016) 79894–79899. https://doi.org/10.1039/c6ra17794h.

[3] I. Kiersztyn, L. Neto, A. Carneiro, J. Tedim, C. Freire, A.R. Hillman, Ion recognition properties of poly[Cu(3-MeOsalpd)] films, Journal of Solid State Electrochemistry. 16 (2012) 2849–2860. https://doi.org/10.1007/s10008-012-1698-3.

[4] M. Nunes, M. Araújo, J. Fonseca, C. Moura, R. Hillman, C. Freire, High-Performance Electrochromic Devices Based on Poly[Ni(salen)]-Type Polymer Films, ACS Applied Materials and Interfaces. 8 (2016) 14231–14243. https://doi.org/10.1021/acsami.6b01977.

[5] K. Łępicka, P. Pieta, G. Francius, A. Walcarius, W. Kutner, Structure-reactivity requirements with respect to nickel-salen based polymers for enhanced electrochemical stability, Electrochimica Acta. 315 (2019) 75–83. https://doi.org/10.1016/j.electacta.2019.05.075.

[6] M. Sukwattanasinitt, A. Nantalaksakul, A. Potisatityuenyong, T. Tuntulani, O. Chailapakul, N. Praphairakait, An Electrochemical Sensor from a Soluble Polymeric Ni-salen Complex, Chemistry of Materials. 15 (2003) 4337–4339. https://doi.org/10.1021/cm034428j.

[7] M.F.S. Teixeira, T.R.L. Dadamos, An electrochemical sensor for dipyrone determination based on nickel-salen film modified electrode, in: Procedia Chemistry, 2009: pp. 297–300. https://doi.org/10.1016/j.proche.2009.07.074.

[8] M. Nunes, M. Araújo, R. Bacsa, R.V. Ferreira, E. Castillejos, P. Serp, A.R. Hillman, C. Freire, N-doped few-layered graphene-polyNi complex nanocomposite with excellent electrochromic properties, Carbon N Y. 120 (2017) 32–43. https://doi.org/10.1016/j.carbon.2017.05.001.

[9] Z. Song, H. Zhou, Towards sustainable and versatile energy storage devices: an overview of organic electrode materials, Energy & Environmental Science. 6 (2013) 2280–2301. https://doi.org/10.1039/c3ee40709h.

[10] I.A. Chepurnaya, M.P. Karushev, E.V. Alekseeva, D.A. Lukyanov, O.V. Levin, Redox-conducting polymers based on metal-salen complexes for energy storage applications, Pure and Applied Chemistry. 92 (2020) 1239–1258. https://doi.org/10.1515/pac-2019-1218.

[11] S.N. Eliseeva, E.V. Alekseeva, A.A. Vereshchagin, A.I. Volkov, P.S. Vlasov, A.S. Konev, O.V. Levin, Nickel-Salen Type Polymers as Cathode Materials for Rechargeable Lithium Batteries, Macromolecular Chemistry and Physics. 218 (2017). https://doi.org/10.1002/macp.201700361.

[12] A.A. Vereshchagin, D.A. Lukyanov, I.R. Kulikov, N.A. Panjwani, E.A. Alekseeva, J. Behrends, O.V. Levin, The Fast and the Capacious: A [Ni(Salen)]-TEMPO Redox-Conducting Polymer for Organic Batteries, Batteries and Supercaps. 4 (2021) 336–346. https://doi.org/10.1002/batt.202000220.

[13] M. Vilas-Boas, I.C. Santos, M.J. Henderson, C. Freire, A.R. Hillman, E. Vieil, Electrochemical behavior of a new precursor for the design of poly[Ni(salen)]-based modified electrodes, Langmuir. 19 (2003) 7460–7468. https://doi.org/10.1021/la034525r.

[14] V.V. Sizov, M.V. Novozhilova, E.V. Alekseeva, M.P. Karushev, A.M. Timonov, S.N. Eliseeva, A.A. Vanin, V.V. Malev, O.V. Levin, Redox transformations in electroactive polymer films derived from complexes of nickel with SalEn-type ligands: computational, EQCM, and spectroelectrochemical study, Journal of Solid State Electrochemistry. 19 (2014) 453–468. https://doi.org/10.1007/s10008-014-2619-4.

[15] D. Larcher, J.M. Tarascon, Towards greener and more sustainable batteries for electrical energy storage, Nature Chemistry. 7 (2015) 19–29. https://doi.org/10.1038/nchem.2085.

[16] E. Kriván, C. Visy, J. Kankare, Key role of the desolvation in the achievement of the quasi-metallic state of electronically conducting polymers, Electrochimica Acta. 50 (2005) 1247–1254. https://doi.org/10.1016/j.electacta.2004.07.050.

[17] L. Niu, C. Kvarnström, A. Ivaska, Mixed ion transfer in redox processes of poly(3,4-ethylenedioxythiophene), Journal of Electroanalytical Chemistry. 569 (2004) 151–160. https://doi.org/10.1016/j.jelechem.2004.01.029.

[18] A. Ispas, R. Peipmann, A. Bund, I. Efimov, On the p-doping of PEDOT layers in various ionic liquids studied by EQCM and acoustic impedance, Electrochimica Acta. 54 (2009) 4668–4675. https://doi.org/10.1016/j.electacta.2009.03.056.

[19] C. Weidlich, K.M. Mangold, K. Jüttner, EQCM study of the ion exchange behaviour of polypyrrole with different counterions in different electrolytes, Electrochimica Acta. 50 (2005) 1547–1552. https://doi.org/10.1016/j.electacta.2004.10.032.

[20] J. Heinze, B.A. Frontana-Uribe, S. Ludwigs, Electrochemistry of conducting polymers-persistent models and new concepts, Chemical Reviews. 110 (2010) 4724–4771. https://doi.org/10.1021/cr900226k.

[21] P.M. Dziewoński, M. Grzeszczuk, Impact of the electrochemical porosity and chemical composition on the lithium ion exchange behavior of polypyrroles (ClO_4^-, TOS^-, $TFSI^-$) prepared electrochemically in propylene carbonate. Comparative EQCM, EIS and CV studies, Journal of Physical Chemistry B. 114 (2010) 7158–7171. https://doi.org/10.1021/jp100796a.

[22] A.R.F. Al-Betar, P.G. Pickup, Influence of counterion charge on the electrochemistry and impedance of polypyrrole, Journal of Solid State Electrochemistry. 24 (2020) 2741–2749. https://doi.org/10.1007/s10008-020-04575-5.

[23] M.A. Vorotyntsev, E. Vieil, J. Heinze, Charging process in polypyrrole films: Effect of ion association, Journal of Electroanalytical Chemistry. 450 (1998) 121–141. https://doi.org/10.1016/S0022-0728(97)00623-2.

[24] A.R. Hillman, M.A. Mohamoud, Ion, solvent and polymer dynamics in polyaniline conducting polymer films, Electrochimica Acta. 51 (2006) 6018–6024. https://doi.org/10.1016/j.electacta.2005.11.054.

[25] T. Fujinami, R. Kinoshita, H. Kawashima, N. Matsumoto, J.H. Harrowfield, Y. Kim, Inclusion complexes of sodium perchlorate into [CuLSS] and [CuLrac]; H2LSS= bis(3-methoxy-2-hydroxy-1- benzylidene)-1S,2S-cyclohexanediamine, H2Lrac= its racemic form,

Journal of Inclusion Phenomena and Macrocyclic Chemistry. 71 (2011) 463–469. https://doi.org/10.1007/s10847-011-9980-z.

[26] A. Bhunia, P.W. Roesky, Y. Lan, G.E. Kostakis, A.K. Powell, Salen-Based infinite coordination polymers of nickel and copper, Inorganic Chemistry. 48 (2009) 10483–10485. https://doi.org/10.1021/ic9017097.

[27] J. Tedim, A. Carneiro, R. Bessada, S. Patrício, A.L. Magalhães, C. Freire, S.J. Gurman, A.R. Hillman, Correlating structure and ion recognition properties of [Ni(salen)]-based polymer films, Journal of Electroanalytical Chemistry. 610 (2007) 46–56. https://doi.org/10.1016/j.jelechem.2007.06.025.

[28] R.V. Apraksin, Y.A. Volosatova, A.I. Volkov, P.S. Vlasov, D.A. Lukyanov, I.R. Kulikov, S.N. Eliseeva, O.V. Levin, Electrochemical synthesis and characterization of poly [Ni(CH_3Osalen)] with immobilized poly(styrenesulfonate) anion dopants, Electrochimica Acta. 368 (2021) 137637. https://doi.org/10.1016/j.electacta.2020.137637.

[29] R.H. Holm, G.W. Everett, A. Chakravorty, Metal Complexes of Schiff Bases and β-Ketoamines, in: K.D. Karlin (Ed.), Progress in Inorganic Chemistry, John Wiley & Sons, Inc., Hoboken, NJ, USA, 1966: pp. 83–214. https://doi.org/10.1002/9780470166086.ch3.

[30] A.R. Hillman, D.C. Loveday, S. Bruckenstein, A general approach to the interpretation of electrochemical quartz crystal microbalance data, Journal of Electroanalytical Chemistry and Interfacial Electrochemistry. 300 (1991) 67–83. https://doi.org/10.1016/0022-0728(91)85384-2.

[31] F. Crameri, Scientific colour maps, (2021). https://doi.org/10.5281/zenodo.5501399.svg.

[32] F. Crameri, G.E. Shephard, P.J. Heron, The misuse of colour in science communication, Nature Communications. 11 (2020) 5444. https://doi.org/10.1038/s41467-020-19160-7.

[33] QCM200 Quartz Crystal Microbalance Digital Controller: Operation and Service Manual, Stanford Research Systems. Revision 2 (2018).

[34] M. Nunes, C. Moura, A.R. Hillman, C. Freire, Novel hybrid based on a poly[Ni(salen)] film and WO_3 nanoparticles with electrochromic properties, Electrochimica Acta. 238 (2017) 142–155. https://doi.org/10.1016/j.electacta.2017.04.010.

[35] D. Tomczyk, W. Bukowski, K. Bester, P. Urbaniak, P. Seliger, G. Andrijewski, S. Skrzypek, The mechanism of electropolymerization of nickel(II) salen type complexes, New Journal of Chemistry. 41 (2017) 2112–2123. https://doi.org/10.1039/c6nj03635j.

[36] J. Tedim, S. Patrício, J. Fonseca, A.L. Magalhães, C. Moura, A.R. Hillman, C. Freire, Modulating spectroelectrochemical properties of [Ni(salen)] polymeric films at molecular level, Synthetic Metals. 161 (2011) 680–691. https://doi.org/10.1016/j.synthmet.2011.01.014.

[37] P. Bhowmik, S. Chatterjee, S. Chattopadhyay, 915708, 915708: Experimental Crystal Structure Determination. (2013).

[38] V.-T. Gruia, A. Ispas, I. Efimov, A. Bund, Cation exchange behavior during the redox switching of poly(3,4-ethylenedioxythiophene) films, Journal of Solid State Electrochemistry. 24 (2020) 3231–3244. https://doi.org/10.1007/s10008-020-04809-6.

[39] H.K. Ismail, H.F. Alesary, A.Y.M. Al-Murshedi, J.H. Kareem, Ion and solvent transfer of polyaniline films electrodeposited from deep eutectic solvents via EQCM, Journal of Solid State Electrochemistry. 23 (2019) 3107–3121. https://doi.org/10.1007/s10008-019-04415-1.

[40] A.R. Hillman, S.J. Daisley, S. Bruckenstein, Solvent effects on the electrochemical p-doping of PEDOT, Physical Chemistry Chemical Physics. 9 (2007) 2379. https://doi.org/10.1039/b618786b.

[41] A.R. Hillman, S.J. Daisley, S. Bruckenstein, Ion and solvent transfers and trapping phenomena during n-doping of PEDOT films, Electrochimica Acta. 53 (2008) 3763–3771. https://doi.org/10.1016/j.electacta.2007.10.062.

[42] M. Vilas-Boas, M.J. Henderson, C. Freire, A.R. Hillman, E. Vieil, A combined electrochemical quartz-crystal microbalance probe beam deflection (EQCM-PBD) study of solvent and ion transfers at a poly[Ni(saltMe)]-modified electrode during redox switching, Chemistry - A European Journal. 6 (2000) 1160–1167. https://doi.org/10.1002/(SICI)1521-3765(20000403)6:7<1160::AID-CHEM1160>3.3.CO;2-U.

[43] G. Zotti, S. Zecchin, G. Schiavon, A. Berlin, Low-Defect Neutral, Cationic, and Anionic Conducting Polymers from Electrochemical Polymerization of N- Substituted Bipyrroles. Synthesis, Characterization, and EQCM Analysis, Chemistry of Materials. 14 (2002) 3607–3614. https://doi.org/10.1021/cm0200386.

[44] J. Widera, M. Skompska, K. Jackowska, The influence of anions on formation, electroactivity, stability and morphology of poly(o-methoxyaniline) films—EQCM studies, Electrochimica Acta. 46 (2001) 4125–4131. https://doi.org/10.1016/S0013-4686(01)00709-5.

[45] E.V. Alekseeva, I.A. Chepurnaya, V.V. Malev, A.M. Timonov, O.V. Levin, Polymeric nickel complexes with salen-type ligands for modification of supercapacitor electrodes: impedance studies of charge transfer and storage properties, Electrochimica Acta. 225 (2017) 378–391. https://doi.org/10.1016/j.electacta.2016.12.135.

[46] Y.A. Oliveira, A. Olean-Oliveira, M.F.S. Teixeira, Short communication: Molecular architecture based on palladium-salen complex/graphene for low potential water oxidation, Journal of Electroanalytical Chemistry. 880 (2021). https://doi.org/10.1016/j.jelechem.2020.114928.

[47] M.F. Mathias, O. Haas, An alternating current impedance model including migration and redox-site interactions at polymer-modified electrodes, The Journal of Physical Chemistry. 96 (1992) 3174–3182. https://doi.org/10.1021/j100186a073.

[48] A.A. Petrov, D.A. Lukyanov, O.A. Kopytko, J.V. Novoselova, E.V. Alekseeva, O.V. Levin, Inversion of the Photogalvanic Effect of Conductive Polymers by Porphyrin Dopants, Catalysts. 11 (2021) 729. https://doi.org/10.3390/catal11060729.

[49] E.V. Beletskii, E.V. Alekseeva, O.V. Levin, Variable-resistance materials for lithium-ion batteries, Russian Chemical Reviews. 91 (2022) RCR5030. https://doi.org/10.1070/RCR5030.

[50] G. Yan, J. Li, Y. Zhang, F. Gao, F. Kang, Electrochemical polymerization and energy storage for poly[Ni(salen)] as supercapacitor electrode material, Journal of Physical Chemistry C. 118 (2014) 9911–9917. https://doi.org/10.1021/jp500249t.

[51] C. O'Meara, M.P. Karushev, I.A. Polozhentceva, S. Dharmasena, H. Cho, B.J. Yurkovich, S. Kogan, J.-H. Kim, Nickel–Salen-Type Polymer as Conducting Agent and Binder for Carbon-Free Cathodes in Lithium-Ion Batteries, ACS Applied Materials & Interfaces. 11 (2019) 525–533. https://doi.org/10.1021/acsami.8b13742.